Dalton Transactions

PAPER

View Article Online
View Journal | View Issue

Cite this: *Dalton Trans.*, 2019, **48**, 15888

Structural isomerism in the $[(Ni@Sn_9)In(Ni@Sn_9)]^{5-}$ Zintl ion†

Chao Zhang,‡[a] Harry W. T. Morgan, ‡[b] Zi-Chuan Wang, ‡[a] Chao Liu,[c] Zhong-Ming Sun *[a] and John E. McGrady *[b]

Received 22nd July 2019,
Accepted 27th September 2019

DOI: 10.1039/c9dt03008e

rsc.li/dalton

A new Zintl cluster, $[(Ni@Sn_9)In(Ni@Sn_9)]^{5-}$, has been isolated in two distinct isomeric forms, one where both $Ni@Sn_9$ units are coordinated to the bridging In atom in an η^3- mode, the other where one is η^3- and the other η^4-. Density functional theory indicates that the energetic separation between these two structures is minimal, suggesting that crystal packing plays a decisive role in the structural chemistry. A comparison of the electronic structure of $[(Ni@Sn_9)In(Ni@Sn_9)]^{5-}$ with $[(Ni@Ge_9)Ni(Ni@Ge_9)]^{4-}$, which has four fewer valence electrons, sheds some light on possible mechanisms that lead to the fusion of cluster fragments.

Introduction

Over the past decade, the reactions of homo-atomic Zintl anions with various sources of transition or main-group metals have emerged as a powerful tool for generating structurally well-defined hetero-metallic clusters.[1] These complex clusters challenge our understanding of chemical bonding and may, ultimately, present new opportunities for rational design of cluster catalysts and quantum dots. Clusters of the heavier group 14 elements (Si, Ge, Sn, Pb) have been particularly prominent, and the nona-tetrelide anions, $[E_9]^{q-}$ (E = Si–Pb, q = 2, 3 or 4), have proven to be ideal precursors for the synthesis of a variety of cluster derivatives.[2] For example, $[Ge_9]^{4-}$ clusters can be coupled and polymerized *via* oxidative coupling to form dimers,[3] oligomers,[4,5] infinite polymers[6] and even mesoporous Ge.[7] Controlled polymerization in the presence of other metals has also been found to give rise to species based on E_9 building blocks, covalently linked by heteroatoms. In the remarkable $[Au_3Ge_{45}]^{9-}$ anion, for example, four polyhedral Ge_9 clusters are linked *via* nine further Ge atoms and three bridging Au^+ ions.[8] More commonly, the bridging heteroatom occupies one vertex of expanded 10-vertex polyhedra, as for example in $[(Ge_9)M(Ge_9)]^{q-}$ (M = Cu, Zn, In, Sn),[9] $[(Sn_9)M(Sn_9)]^{q-}$ (M = Ag, Hg)[10] (a/b and c in Fig. 1, respectively) and $[MGe_{18}\{Si(SiMe_3)_3\}_6]^{q-}$ (M = Au, Zn, Cd, Hg).[11] Of particular relevance to this work is the structural chemistry of $[(Ge_9)Zn(Ge_9)]^{6-}$, which crystallises in two distinct isomers depending on the number of molecules of NH_3 in the unit cell. In one case both Ge_9 units coordinate *via* triangular faces (η^3:η^3 coordination, a in Fig. 1)

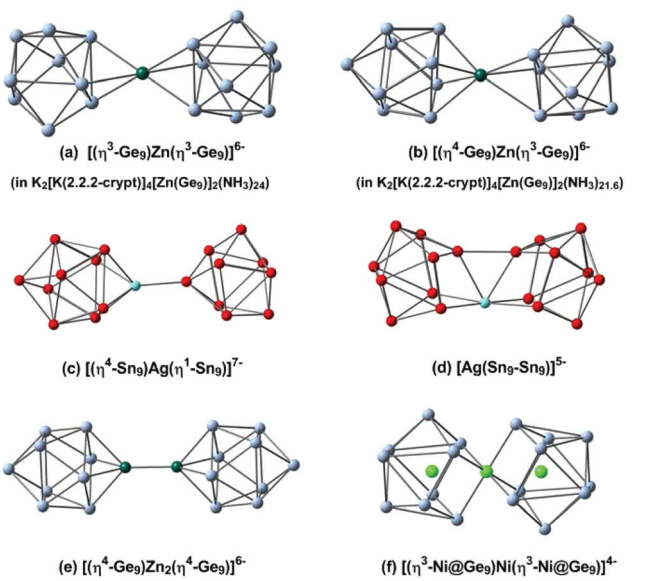

Fig. 1 η^3:η^3, η^4:η^3 and η^4:η^1 isomers of known hetero-atom-bridged Zintl-ion clusters, (a) $[(\eta^3\text{-}Ge_9)Zn(\eta^3\text{-}Ge_9)]^{6-}$; (b) $[(\eta^4\text{-}Ge_9)Zn(\eta^3\text{-}Ge_9)]^{6-}$; (c) $[(\eta^4\text{-}Sn_9)Ag(\eta^3\text{-}Sn_9)]^{7-}$; (d) $[Ag(Sn_9\text{-}Sn_9)]^{5-}$; (e) $[(\eta^4\text{-}Ge_9)Zn_2(\eta^4\text{-}Ge_9)]^{6-}$; (f) $[(\eta^3\text{-}Ni@Sn_9)Ni(\eta^3\text{-}Ni@Sn_9)]^{4-}$.

[a]*School of Materials Science and Engineering, State Key Laboratory of Elemento-Organic Chemistry, Tianjin Key Lab for Rare Earth Materials and Applications, Nankai University, Tianjin 300350, China. E-mail: sunlab@nankai.edu.cn*
[b]*Department of Chemistry, University of Oxford, Oxford, OX1 3QZ, UK. E-mail: john.mcgrady@chem.ox.ac.uk*
[c]*College of Chemistry and Chemical Engineering, Central South University, Changsha, 410083, People's Republic of China*

†Electronic supplementary information (ESI) available: X-ray crystallographic file in CIF format, full experimental and computational details as well as ESI-MS spectra. CCDC 1941744 and 1941745. For ESI and crystallographic data in CIF or other electronic format see DOI: 10.1039/c9dt03008e

‡These authors contributed equally.

while in the other, one Ge_9 unit is η^3 and the other η^4 (b in Fig. 1). The $[(\eta^4\text{-}Sn_9)Ag(\eta^1\text{-}Sn_9)]^{7-}$ anion (c) presents a third coordination mode, where the Sn_9 units are bonded to the Ag^+ ion *via* either a square face or a single Sn atom.[10a] Trimeric $[(Ge_9)Zn(Ge_9)Zn(Ge_9)]^{8-}$,[12] tetrameric $[Hg_3(Ge_9)_4]^{10-}$,[13] and even polymeric $^{\infty}[M(Ge_9)]^{2-}$ (M = Zn, Hg),[14] species have also been synthesised. Clusters linked by dimer (M_2) and trimer (M_3) units are also well established, examples including $[(Ge_9)Zn\text{-}Zn(Ge_9)]^{6-}$ (e in Fig. 1)[12] $[(Ge_9)Cd\text{-}Cd(Ge)_9]^{6-}$,[15] $[(Ge_9)Au_3(Ge)_9]^{5-}$,[16] and $[(Ni(CO)_2)_2(u\text{-}Si_9)_2]^{8-}$.[17]

In all the examples noted in the previous paragraph the E_9 units are empty, but there is a closely related family of compounds based on clusters containing an endohedral metal ion. For germanium-based clusters, this family includes $[Ni@Ge_9]^{q-}$,[18] $[M@Ge_{10}]^{3-}$ (M = Co, Fe)[19] and $[Ru@Ge_{12}]^{3-}$,[20] as well as multimetallic $[Co_2@Ge_{16}]^{4-}$,[21] $[Pd_2@Ge_{18}]^{4-}$,[22] and $[Ni_3@Ge_{18}]^{4-}$ (f in Fig. 1).[18b] Amongst the heavier congeners, Sn and Pb, known examples include $[M@Sn_9]^{4-}$, (M = Co, Ni),[18,23] $[Cu@E_9]^{3-}$ (E = Sn, Pb),[24] $[Ni@Pb_{10}]^{2-}$,[25] $[M@Pb_{12}]^{2-}$, (M = Ni, Pd, Pt, Mn)[26] and $[Ir@Sn_{12}]^{3-}$.[27] Multimetallic $[M_2@Sn_{17}]^{q-}$ (M = Ni, Co, Pt, Rh)[28–30] and $[Pd_2@Sn_{18}]^{4-}$,[31] are also known, along with the recently reported tri-rhodium cluster $[Rh_3@Sn_{24}]^{5-}$.[30] Despite this wealth of crystallographic data, the precise mechanisms by which these clusters form from their smaller component parts remain an open question, largely because the reactions are rarely stoichiometric and the isolation of the intrinsically very reactive intermediates is challenging.[32]

In this paper, we describe synthetic methods that lead to two distinct isomers of the indium-bridged endohedral cluster, $[(Ni@Sn_9)In(Ni@Sn_9)]^{5-}$. The two isomers are isostructural with the two forms of $[(Ge_9)Zn(Ge_9)]^{5-}$ shown in Fig. 1a and b, but the E_9 units now contain an endohedral metal. Clusters of this type are in fact remarkably rare, and, amongst the species described in the previous paragraph, only $[Ni_3@Ge_{18}]^{4-}$ can be considered as a direct endohedral analogue of the extensive $(E_9)M(E_9)$ family. The relative dearth of clusters of the $[(M@E_9)M'(M@E_9)]$ type may well reflect the strong repulsions between endohedral M and bridging M′ atoms at the very short separations (typically 2.5–2.8 Å) imposed by the geometry of the cluster. In a recent study of ternary functionalized $[Co@Sn_9]^{4-}$ clusters, $[Co@Sn_9(ML)]^{4-}$, we showed that these repulsions can destabilize the Co–M σ* orbital to the extent that the electrons are transferred into a cluster-based orbital with concomitant formation of a Co–M bond.[33] The redox ambiguity of E_9 cages is well established, and Ge_9 has been isolated in the 2−, 3− and 4− charge states.[34] Thus it is possible to conceive a range of plausible formulations for $[Ni_3@Ge_{18}]^{4-}$ ranging from $[Ni_3]^0([Ge_9]^{2-})_2$ to $[Ni_3]^{2+}([Ge_9]^{3-})_2$ to $[Ni_3]^{4+}([Ge_9]^{4-})_2$. The presence of an In centre in the bridging position in $[(Ni@Sn_9)In(Ni@Sn_9)]^{5-}$ will alter the balance between M–M′ and E–E bonding, and so, by comparing the electronic structures of $[(Ni@Sn_9)In(Ni@Sn_9)]^{5-}$ and $[(Ni@Ge_9)Ni(Ni@Ge_9)]^{4-}$, we hope to shed some light on the interplay between metal–metal and tetrel–tetrel bonding in these clusters.

Experimental section

General synthetic methods

All manipulations and reactions were performed in a nitrogen atmosphere using standard Schlenk or glovebox techniques. The intermetallic precursors, $K_4Ni_3Sn_9$ and K_4Sn_9 were synthesized according to previously reported procedures from stoichiometric mixtures of the elements (K: 99.95%, Aldrich; Sn: 99.8%, Strem, Ni: 99.95%) heated to 1000 °C for 72 h in sealed niobium containers.[35] [2.2.2]-Crypt (4,7,13,16,21,24-hexaoxa-1,10-diazabicyclo [8.8.8] hexacosane, purchased from Sigma-Aldrich (98%) was dried under a vacuum for 1 day prior to use. $In(C_6H_5)_3$ was prepared according to a literature procedure. $Ni(COD)_2$ (COD = cyclo-octadiene) (Strem, 98%) is used as received after careful drying under a vacuum. Ethylenediamine (en) (Aldrich, 99%), *N*,*N* dimethylformamide (DMF), and acetonitrile (MeCN) were freshly distilled over CaH_2 prior to use. Toluene (tol) (Aldrich, 99.8%) was distilled from sodium/benzophenone and stored under inert atmosphere (N_2).

X-ray crystal structure determination

Suitable crystals were selected for single-crystal X-ray diffraction analyses. Crystallographic data were collected on a Bruker Apex II CCD diffractometer with graphite-monochromated Mo Kα radiation (λ = 0.71073 Å). Data processing was accomplished with the SAINT program. Structures were solved using direct methods (SHELXT, Olex2) and then refined using SHELXL-2014 and Olex2 to convergence,[36] in which all of the non-hydrogen atoms were refined anisotropically. Non-hydrogen atoms were refined with anisotropic displacement parameters during the final cycles. All hydrogen atoms of the organic molecule were placed by geometrical considerations and were added to the structure factor calculation. A summary of the crystallographic data for these two complexes is listed in Table 1. Selected bond distances and angles are given in Tables S1–S2.† CCDC entries 1941744 and 1941745† contain the supplementary crystallographic data for this paper.

Mass spectrometry

Electrospray ionization mass spectrometry (ESI-MS) was performed in negative-ion mode on an LTQ linear ion trap spectrometer. The spray voltage was 5.48 kV and the capillary temperature was kept at 300 °C. The capillary voltage was 30 V. The samples were made up inside a glovebox under an inert atmosphere and transferred to the spectrometer in an airtight syringe using a Harvard syringe pump at 15 μL min^{-1}.

Synthesis of $[K(2,2,2\text{-crypt})]_5[Ni@Sn_9]In[Ni@Sn_9]$, 1

$K_4Ni_3Sn_9$ (140 mg, 0.1 mmol) and 2,2,2-crypt (150 mg, 0.4 mmol) were dissolved in DMF (2 mL) in a test tube and stirred. After 30 min $In(C_6H_5)_3$ (69 mg, 0.2 mmol) was added directly to the solution. The resulting dark-red solution was stirred for an additional 2.5 h and was then centrifuged and filtered. The resulting solution was layered with toluene. Black block shaped crystals were obtained after one week (122 mg, 61% crystalline yield, based on the Sn content of the starting material, $K_4Ni_3Sn_9$).

Table 1 X-ray measurements and structure solution of compound **1** and **2**

Compound	**1**	**2**
Empirical formula	$C_{66}H_{150}O_{30}N_6K_5Ni_2InSn_{18}$	$C_{93}H_{187}O_{31}N_{11}K_5Ni_2InSn_{18}$
Formula weight	4072.42 g mol^{-1}	4520.04 g mol^{-1}
Crystal system	Monoclinic	Triclinic
Space group	$P2_1/c$	$P\bar{1}$
a/Å	20.016(4)	14.3638(17)
b/Å	15.269(3)	23.353(3)
c/Å	42.228(7)	25.857(3)
α/°	90	67.719(2)
β/°	105.883(8)	74.380(2)
γ/°	90	75.977(2)
V	12 413(4)	7633.0(16)
Z	4	1
ρ_{calc} /g cm^{-3}	2.092	3.583
μ(MoKα)/mm^{-1}	4.248	10.044
F(000)	7088.0	7392.0
2Θ range/°	2.85–49.996	2.98–50
Reflections collected/unique	67 185	26 650
Data/restraints/parameters	21 704/143/1153	26 650/60/1452
R_1/wR_2 ($I > 2\sigma(I)$)[a]	0.0704/0.1505	0.0701/0.1787
R_1/wR_2 (all data)	0.1483/0.1751	0.1356/0.2039
GooF (all data)[b]	1.019	0.937
Data completeness	0.99	0.99
Max. peak/hole /e$^-$ Å^{-3}	2.114/−2.504	2.618/−1.744

[a] $R_1 = \sum||F_o| - |F_c||/\sum|F_o|$; $wR_2 = \{\sum w[(F_o)^2 - (F_c)^2]^2/\sum w[(F_o)^2]^2\}^{1/2}$. [b] GooF = $\{\sum w[(F_o)^2 - (F_c)^2]^2/(n-p)\}^{1/2}$.

Synthesis of [K(18-crown-6)]$_5$[Ni@Sn$_9$]In[Ni@Sn$_9$], 2

K_4Sn_9 (123 mg, 0.1 mmol), $In(C_6H_5)_3$ (69 mg, 0.2 mmol) and 18-crown-6 (106 mg, 0.4 mmol) were dissolved in en (2 mL) in a test tube and stirred for 30 min. After 30 min $Ni(COD)_2$ (55 mg, 0.2 mmol) was added directly to the solution. The resulting dark-red solution was stirred for an additional 2.5 h and was then centrifuged and filtered. The resulting solution was layered with toluene. Large, black stripe shaped crystals were obtained after one week (68 mg, 31% crystalline yield based on the Sn content of the starting material, K_4Sn_9).

Quantum chemical investigations

DFT calculations were performed with the ORCA software package (version 4.1.1)[37] using the BP86 functional[38] along with ma-def2-TZVP basis sets on Ni/In and ma-def2-SVP on Sn/Ge.[39] The core electrons of In and Sn were modelled with the 28-electron ECPs of Dolg.[40] Calculations were accelerated by means of the Resolution of Identity (RI) approximation[41] with the def2/J auxiliary basis set.[42] The confining influence of the crystalline environment was approximated using a Conductor-like Polarizable Continuum Model (CPCM) with the dielectric constant of water.[43] The geometries were fully optimized, and confirmed to be local minima by the absence of imaginary vibrational frequencies.

Results and discussion

We report here two quite distinct synthetic protocols, both of which generate the $[(Ni@Sn_9)In(Ni@Sn_9)]^{5-}$ anion, but in different isomeric forms. The first route, leading to **1**, involves adding a source of In^{3+} ($In(C_6H_5)_3$) to a pre-formed solution of the endohedral $[Ni@Sn_9]^{3-}$ anion in DMF. $[(Ni@Sn_9)In(Ni@Sn_9)]^{5-}$ is then crystallised as its $[K(2,2,2\text{-crypt})]^+$ salt. In the second protocol, leading to **2**, a source of Sn (K_4Sn_9) is first mixed with $In(C_6H_5)_3$, at which point a range of anionic species including $[Sn_9In]^-$ and $[Sn_9In(C_6H_5)]^-$ is present in solution. Addition of a source of Ni^0 ($Ni(COD)_2$) then generates the same $[(Ni@Sn_9)In(Ni@Sn_9)]^{5-}$ anion, this time isolated as its $[K(18\text{-C-}6)]^+$ salt in **2**. The negative ion mode ESI-MS of freshly dissolved crystalline samples of **1** and **2** in CH_3CN reveal extensive fragmentation that is typical of clusters of this type (Fig. 2). The spectra of the two compounds clearly show a signal corresponding to the 4-electron oxidized molecular ion $\{[Ni@Sn_9]In[Ni@Sn_9]\}^-$ (m/z = 2368.01) but also a stronger signal corresponding to $[NiSn_9In]^-$ (m/z = 1241.96). Peaks arising from $[NiSn_9]$ units, either in isolation or in ion pairs were also detected ($\{[K(2,2,2\text{-crypt})][NiSn_9]\}^-$, m/z = 1542.25 and $\{[K(18\text{-C-}6)][NiSn_9]\}^-$, m/z = 1430.17) The relative abundance of peaks corresponding to In-containing clusters indicates that the In ions are strongly bound to the cluster. In addition, weak signals for the Ni-free species $\{[K(2,2,2\text{-crypt})]_2[Sn_9]\}^-$ were also observed in the spectrum of compound **1**.

X-ray diffraction reveals that the presence of different counter-ions in **1** and **2** ($[K(2,2,2\text{-crypt})]^+$ and $[K(18\text{-C-}6)]^+$, respectively) leads to different isomers of the penta-anionic cluster $[(Ni@Sn_9)In(Ni@Sn_9)]^{5-}$ (Fig. 3). Full details of bond lengths are given in ESI, Table S1.† In **1**, both $Ni@Sn_9$ units are coordinated to the bridging indium atom in η^3 coordination mode, similar to those observed in $[(\eta^3\text{-}Ge_9)In(\eta^3\text{-}Ge_9)]^{5-}$ and $[(\eta^3\text{-}Ge_9)Zn(\eta^3\text{-}Ge_9)]^{6-}$.[7c,a] Both $[Ni@Sn_9]^{4-}$ subunits in **1**

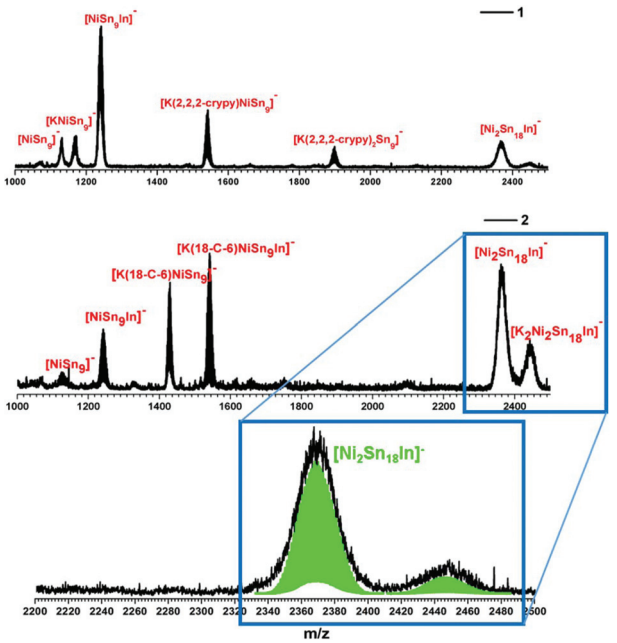

Fig. 2 Negative ion mode ESI-MS (*m*/*z*: 1000–2500) of a freshly dissolved crystalline sample of **1** (top) and **2** (bottom) in CH_3CN. The green spectrum shows the simulated spectra of $[Ni_2Sn_{18}In]^-$ and $[K_2Ni_2Sn_{18}In]^-$ superimposed on the expansion of the high-mass region for **2**.

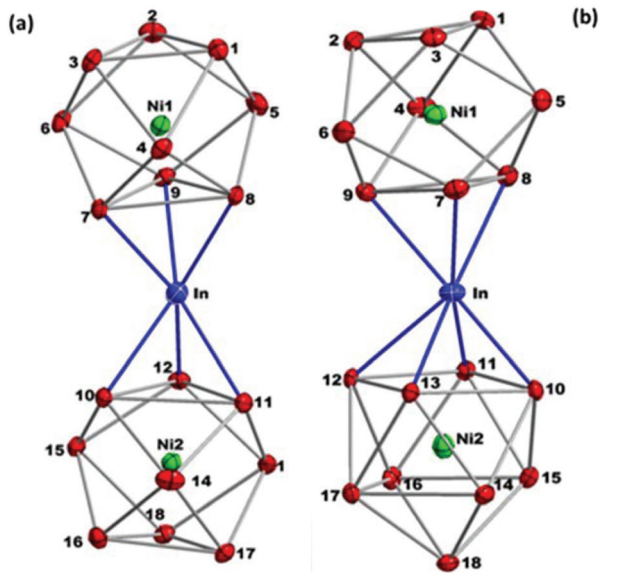

Fig. 3 ORTEP plots of the $[(Ni@Sn_9)In(Ni@Sn_9)]^{5-}$ anions in **1** (a) and **2** (b) (drawn at 50% probability). Selected distances [Å] in **1**: Sn(7)–In(1) 3.0542, Sn(8)–In(1) 3.0508, Sn(9)–In(1) 3.1143, Sn(10)–In(1) 3.0981, Sn(11)–In(1) 3.1252, Sn(12)–In(1) 2.9949, Sn(7)–Sn(8) 3.2797, Sn(8)–Sn(9) 3.2873, Sn(7)–Sn(9) 3.2704, selected distances [Å] in **2**: Sn(7)–In(1) 3.1691, Sn(8)–In(1) 3.1212, Sn(9)–In(1) 3.1194, Sn(10)–In(1) 2.9916, Sn(11)–In(1) 3.0712, Sn(12)–In(1) 2.3344, Sn(13)–In(1) 3.0484, Sn(7)–Sn(8) 3.2464, Sn(7)–Sn(9), Sn(10)–Sn(11) 3.2132, Sn(11)–Sn(12) 3.0483, Sn(12)–Sn(13) 3.0521, Sn(13)–Sn(10) 3.2324.

(Fig. 3a) are approximately tricapped trigonal prismatic, with Ni–Sn bond lengths in the range 2.521(3) Å to 2.707(3) Å, comparable to those observed in the isolated cluster $[Ni@Sn_9]^{4-}$.[23a] The two triangular faces are almost perfectly eclipsed, giving approximate D_{3h} local symmetry to the cluster, and the In–Sn distances to the coordinated triangular faces lie between 2.9949(17) and 3.1252(17) Å. In contrast, the two $[Ni@Sn_9]^{4-}$ units in **2** adopt η^3- (the upper unit in Fig. 3b) and η^4- (the lower unit) coordination modes. The In–Sn distances in the η^3-coordinated cluster range from 3.1194(21) to 3.1691(18) Å, very similar those in **1**. The η^4-coordinated cluster is a distorted mono-capped square antiprism with approximate local C_{2v} symmetry, and is bonded to the bridging In *via* four Sn atoms of an open square face. The In–Sn distances lie in a similar range, between 2.9916(16) and 3.2344(2) Å. The distortion from perfect four-fold symmetry is most pronounced in the Sn-capped square face (Sn14 to Sn17), where Sn–Sn contacts vary by almost 0.5 Å, between 3.182(2) and 3.640(8) Å. This η^3:η^4 coordination mode is very similar to the $[(\eta^4\text{-}Ge_9)Zn(\eta^3\text{-}Ge_9)]^{6-}$ isomer shown in Fig. 1b, and also to $[(\eta^4\text{-}Ge_9)Sn(\eta^3\text{-}Ge_9)]^{4-}$, also reported by Bentlohner *et al.*[9a] Their detailed electronic structure analysis suggests that the approximately C_{4v}-symmetric $[Ge_9Sn]^{2-}$ fragment can be considered as a 10-vertex *closo* (22-electron) cluster which donates a Sn lone pair to the LUMO of a *closo* 20-electron $[Ge_9]^{2-}$ unit.[9a] By analogy, the η^3:η^4 isomer of $[(Ni@Sn_9)In(Ni@Sn_9)]^{5-}$ in **2** can be formulated as a *closo* $[Ni@Sn_9In]^{3-}$ unit bound to a tri-capped trigonal prismatic $[Sn_9]^{2-}$ unit. A search of the Cambridge Structural Database reveals only two crystallographically characterized species with covalent In–Sn bonds, both of which are somewhat shorter at 2.8638(7) Å and 2.8886(4) Å.[44] The sum of the Sn and In covalent radii proposed by Alvarez and coworkers is even shorter again, at 2.81 Å,[45] suggesting that the interactions in **1** and **2** are somewhat weaker than a conventional single In–Sn covalent bond.

The pathway that leads to the formation of **1** appears relatively straightforward: two pre-formed $[Ni@Sn_9]^{4-}$ units that are known to be present in solution prior to the addition of $In(C_6H_5)_3$ displace the C_6H_5 ligands. The mechanism that leads to **2**, in contrast, is somewhat less certain since we have been unable to isolate any intermediates from the reaction of $[Sn_9]^{4-}$ and $In(C_6H_5)_3$. One possibility is that **2** is generated by insertion of Ni atoms into a pre-formed $[(Sn_9)In(Sn_9)]^{5-}$ intermediate. This species has not been isolated but it is isoelectronic with the known compound $[(Sn_9)Ag(Sn_9)]^{7-}$ (Fig. 1c) and the ESI-MS of the reaction mixture shows a strong signal assigned to $[Sn_9In]^-$, a plausible fragmentation product of $[(Sn_9)In(Sn_9)]^{5-}$. We also note by way of precedent that the $[Ge_9Sn]^-$ anion is the only species observed when the bridged cluster $[(Ge_9)Sn(Ge_9)]^{4-}$ is analysed using ESI-MS.[7a] Alternatively, it is conceivable that a Ni atom may insert into the $[(Sn_9)In(C_6H_5)]^-$ species (observed in the ESI-MS) prior to formation of the $[(Sn_9)In(Sn_9)]$ unit. This would generate a $[(Ni@Sn_9)In(C_6H_5)]^-$ intermediate which could then coalesce with a further Sn_9 or $Ni@Sn_9$ unit to generate the product.

In order to probe the electronic origins of the isomerism observed in the solid state, we have used density functional

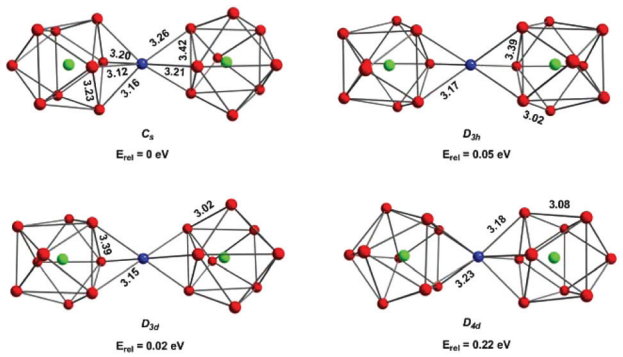

Fig. 4 Optimised structures and energies of the η^4:η^3, η^3:η^3 (eclipsed), η^3:η^3 (staggered) and η^4:η^4 (staggered) isomers of the $[(Ni@Sn_9)In(Ni@Sn_9)]^{5-}$ anion.

theory (BP86, ma-def2-SVP/TZVP basis) to explore the potential energy surface of the $[(Ni@Sn_9)In(Ni@Sn_9)]^{5-}$ anion. In all cases a continuum solvent model (H_2O) was used to approximate the confining effects of the cationic environment in the solid state. We have been able to locate distinct minima with C_s (η^4:η^3) and D_{3h} (η^3:η^3) symmetry, both shown in Fig. 4, with Ni–Sn and In–Sn bond lengths only marginally longer than those in the crystal structures shown in Fig. 3. The C_s-symmetric η^4:η^3 isomer constitutes the global minimum on the gas-phase potential energy surface but the D_{3h}-symmetric alternative lies only 0.05 eV higher. Moreover, a third, D_{3d}-symmetric, isomer where the two η^3-coordinated $Ni@Sn_9$ units are staggered, also lies at very similar energy (+0.02 eV relative to the η^3:η^4 global minimum). The very similar energies and bond lengths for the D_{3h} and D_{3d} isomers suggests that the $Ni@Sn_9$ units will be free to rotate about the Ni–In–Ni axis in solution. All attempts to locate a minimum corresponding to the η^4:η^1 structure adopted by $[(Sn_9)Ag(Sn_9)]^{7-}$ converged back to the C_s-symmetric η^4:η^3 global minimum. A fourth isomer with an η^4:η^4 mode based on vertex-sharing bi-capped square anti-prismatic $Ni@Sn_9In$ units proves to be substantially less stable, and can be safely eliminated. Our survey therefore suggests that the gas-phase potential energy surface is very flat, and that the energetic differences between the C_s, D_{3h} and D_{3d} isomers are well below any reasonable estimate of the intrinsic accuracy of the computational methodology. It seems likely, therefore, that the presence of different isomers of $[(Ni@Sn_9)In(Ni@Sn_9)]^{5-}$ in **1** and **2** reflects subtle differences in the crystalline environment rather than any fundamental differences in bonding that arises from the different synthetic protocols used to generate them.

We have noted above that the $[(Ni@Ge_9)Ni(Ni@Ge_9)]^{4-}$ anion described by Goicoechea and Sevov,[18b] the optimized structure of which is shown in Fig. 5, is isostructural to $[(Ni@Sn_9)In(Ni@Sn_9)]^{5-}$, and so offers a natural point of comparison. The Ni_3 cluster has D_{3d} symmetry, with the two triangular faces of the $Ni@Ge_9$ units forming an approximately octahedral environment around the central Ni. To facilitate a direct comparison between the two clusters we will focus the discussion below on the D_{3d} isomer of $[(Ni@Sn_9)In(Ni@Sn_9)]^{5-}$. A comparison of the optimized structures of the clusters, shown in Fig. 5, highlights the superficial similarities between the two, but also some more subtle differences. The most obvious difference is that the In–Ni separation of 4.18 Å effectively precludes any covalent interaction while the Ni–Ni

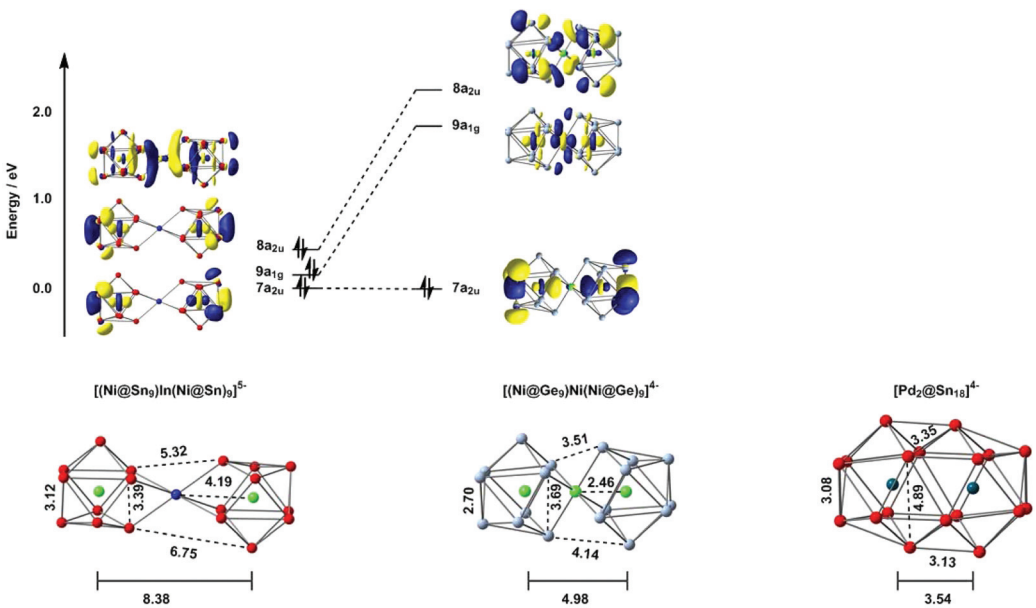

Fig. 5 Optimised structures of $[(Ni@Sn_9)In(Ni@Sn_9)]^{5-}$, $[(Ni@Ge_9)Ni(Ni@Ge_9)]^{4-}$ and $[Pd_2@Sn_{18}]^{4-}$ (D_{3d} isomer in each case) and the frontier Kohn–Sham orbitals of the first two clusters. The $7a_{2u}$ orbital, an out-of-phase combination of Ni $3d_{z^2}$ in each case, is taken as the arbitrary zero on the energy scale.

distance of 2.46 Å in $[(Ni@Ge_9)Ni(Ni@Ge_9)]^{4-}$ is well within bonding range (noting the caveat that the bond length and bond strength are not necessarily strongly correlated due to the constraints imposed by the cage). More subtly, the shape of the triangular faces that coordinate to the bridging In/Ni atoms differ substantially: in $[(Ni@Sn_9)In(Ni@Sn_9)]^{5-}$ the Sn–Sn distances within the faces are short (3.39 Å in Fig. 5) while the distances between nearest neighbors on opposite sides of the bridging In atom are long (5.32 Å), the ratio between the two being 0.64. In contrast, the Ge–Ge distances in the coordinated faces of the Ge_9 clusters in $[(Ni@Ge_9)Ni(Ni@Ge_9)]^{4-}$ are relatively long (3.69 Å), and in fact longer than the nearest-neighbor distances across the equator of the molecule (3.51 Å), a ratio of 1.05. In the D_{3d}-symmetric di-palladium clusters $[Pd_2@Ge_{18}]^{4-}$ and $[Pd_2@Sn_{18}]^{4-}$,[22,31a] where the two E_9 units are completely fused, the corresponding ratio of E–E distances around the central triangular faces to E–E distances across the equator is approximately 1.46 (the structure of $[Pd_2@Sn_{18}]^{4-}$, optimized at the same level of theory, is shown in Fig. 5 for comparison). The structural characteristics of $[(Ni@Ge_9)Ni(Ni@Ge_9)]^{4-}$ therefore seem to place it at an intermediate stage in the coalescence of the two E_9 units, lying almost exactly midway between the completely separated and fully coalesced extremes defined by $[(Ni@Sn_9)In(Ni@Sn_9)]^{5-}$ and $[Pd_2@E_{18}]^{4-}$, respectively.

The total valence electron count at the two clusters differs by 4: $[(Ni@Sn_9)In(Ni@Sn_9)]^{5-}$ has 110 (we include the d^{10} shell of In in the valence manifold) while the $[(Ni@Ge_9)Ni(Ni@Ge_9)]^{4-}$ cluster has only 106, and it is the nature of the orbitals that are occupied in the former but vacant in the latter that hold the key to understanding the differences in structural chemistry. In $[(Ni@Sn_9)In(Ni@Sn_9)]^{5-}$, the $8a_{2u}$ HOMO is an out-of-phase combination of the orbitals that constitute the HOMOs of the two $[Ni@Sn_9]^{4-}$ fragments (the in-phase combination lies lower in energy and is also occupied). The HOMO−1 and HOMO−2 ($9a_{1g}$ and $7a_{2u}$, respectively) are in- and out-of-phase combinations of Ni $3d_{z^2}$ orbitals – all other linear combinations of Ni 3d orbitals are also occupied. The fact that the $8a_{2u}$ orbital is occupied suggests that the two $Ni@Sn_9$ units are in the 4− oxidation state, leaving the central In in the 3+ oxidation state to achieve charge balance.

In their original paper, Goicoechea and Sevov discussed the bonding in terms of a central d^{10} Ni^0 atom interacting with two hypo-electronic $[Ni@Ge_9]^{2-}$ units. More recently, Lin and Sheong have considered the bonding in the context of their mutual delocalization model, and argued similarly that the $[Ni@Ge_9]^{2-}$ units serve as 2-electron donors to the central Ni^0.[46] In terms of the model discussed above, this would imply the removal of two pairs of electrons from orbitals localized on the $[NiGe_9]$ units. Instead, we see that the $9a_{1g}$ orbital, the LUMO of $[(Ni@Ge_9)Ni(Ni@Ge_9)]^{4-}$, has a large amplitude on the central Ni atoms, and the orbital is strongly Ni–Ni antibonding. This implies that the Ni_3 chain as a whole is best regarded as $[Ni_3]^{2+}$, with a 3-centre-4-electron bond delocalized along the Ni_3 chain. The second vacant orbital, the $8a_{2u}$ LUMO+1, is localized almost entirely on the Ge_9 units, suggesting that the two Ge_9 cluster units should be considered as being in the $[Ge_9]^{3-}$ oxidation state, as required for charge balance. The $8a_{2u}$ LUMO+1 has substantial antibonding character between the two triangular faces on opposite sides of the equator of the cluster, indicative of some direct Ge–Ge bonding between the two Ge_9 units. The orbital is, however, delocalized over 6 Ge–Ge nearest neighbor contacts and so the net bond order is only 1/6 per bond, consistent with the rather long Ge–Ge separation of 3.51 Å. The $8a_{2u}$ orbital is also bonding with respect to the three atoms that make up the triangular faces coordinated to the central Ni, and so the removal of two electrons serves to expand these faces, another of the structural features noted above. The structural influence of electrons in this orbital has been discussed previously in the context of isolated E_9 units in the $[Ge_9NiL]^{z-}$ series[34] but in the present case the effect is magnified by the antibonding interactions between the two E_9 units.

Our analysis of the structural data, along with the shape of the vacant orbitals, is consistent with a formulation of the $[(Ni@Ge_9)Ni(Ni@Ge_9)]^{4-}$ cluster as a $[Ni_3]^{2+}$ unit inside a $([Ge_9]^{3-})_2$ cage where the two cluster units are partially fused. It is also worth highlighting here the relationship to the $[Ag(Sn_9)_2]^{7-/5-}$ redox pair reported by Fässler and co-workers, and shown in Fig. 1c/d.[10a,47] The former is valence isoelectronic with $[(Ni@Sn_9)In(Ni@Sn_9)]^{5-}$, and also contains two clearly separated $[Sn_9]^{4-}$ clusters bridged by an Ag^+ ion (in this case in an η^4–η^1 coordination mode). In the latter, in contrast, two formally $[Sn_9]^{3-}$ clusters are fused by a single covalent Sn–Sn bond, and in ref. 10*a* the authors anticipated that a redox cascade starting from $[Ag(Sn_9)_2]^{7-}$ might constitute a viable mechanism for forming Sn–Sn bonds. The difference between $[(Ni@Ge_9)Ni(Ni@Ge_9)]^{4-}$, with six inter-cluster Ge–Ge bonds of order 1/6, and $[Ag(Sn_9)_2]^{5-}$, with a single localized Sn–Sn bond, then lies only in the degree of localization of the bonding between the cluster units. The presence of the 3-centre-4-electron bond in the Ni_3 chain may confer a degree of rigidity that prevents the hinging at the central atom required to localize the bonding in a single Sn–Sn contact.

Conclusions

In summary, we have reported here the synthesis and structural characterisation of a new endohedral bridged Zintl cluster $[(Ni@Sn_9)In(Ni@Sn_9)]^{5-}$, which has been isolated in two distinct isomeric forms that differ in the coordination geometry to the bridging In atom. The co-existence of η^3:η^3 and η^4:η^3 coordination modes of the $Ni@Sn_9$ moieties has precedent in $[(Ge_9)Zn(Ge_9)]^{6-}$, and DFT calculations confirm that the two isomers are almost iso-energetic. An analysis of the electronic structure suggests that $[(Ni@Sn_9)In(Ni@Sn_9)]^{5-}$ can be considered straightforwardly as two $[Ni@Sn_9]^{4-}$ units coordinated to an electronically innocent In^{3+} centre. As such, it provides an important benchmark for the isostructural $[(Ni@Ge_9)Ni(Ni@Ge_9)]^{4-}$ anion, which has four fewer valence electrons and features both Ni–Ni bonding and weak inter-

actions between the Ge atoms on the opposing triangular faces of the Ge_9 units. Structurally and electronically, the $[(Ni@Ge_9)Ni(Ni@Ge_9)]^{4-}$ anion appears to lie midway between $[(Ni@Sn_9)In(Ni@Sn_9)]^{5-}$, where the two Sn_9 cages are clearly separated, and $[Pd_2@Sn_{18}]^{4-}$, where they have coalesced to form a single continuous Sn_{18} cage. This in turn suggests that encapsulated metal ions may play an important templating role in the coalescence of smaller cluster units by depopulating orbitals that are anti-bonding between the separated fragments.

Conflicts of interest

There are no conflicts to declare.

Acknowledgements

This work was supported by the National Natural Science Foundation of China (No. 1971118, 21722106). HWTM thanks the EPSRC for support through the Centre for Doctoral Training, Theory and Modelling in Chemical Sciences, under grant EP/L015722/1, and the Radcliffe scholarship fund at University College, Oxford.

Notes and references

1 (*a*) S. Scharfe, F. Kraus, S. Stegmaier, A. Schier and T. F. Fässler, *Angew. Chem., Int. Ed.*, 2011, **50**, 3630–3670; (*b*) T. F. Fässler, *Struct. Bonding*, 2011, **140**, 91–131; (*c*) R. S. P. Turbervill and J. M. Goicoechea, *Chem. Rev.*, 2014, **114**, 10807–10828; (*d*) B. Weinert and S. Dehnen, *Struct. Bonding*, 2017, **174**, 99–134; (*e*) A. Schnepf, *Chem. Soc. Rev.*, 2007, **36**, 745–758.

2 J. M. Goicoechea and S. C. Sevov, *Organometallics*, 2006, **25**, 4530–4530.

3 (*a*) L. Xu and S. C. Sevov, *J. Am. Chem. Soc.*, 1999, **121**, 9245–9246; (*b*) R. Hauptmann and T. F. Fässler, *Z. Anorg. Allg. Chem.*, 2003, **629**, 2266–2273; (*c*) A. Nienhaus, S. D. Hoffmann and T. F. Fässler, *Z. Anorg. Allg. Chem.*, 2006, **632**, 1752–1758; (*d*) S. Scharfe and T. F. Fässler, *Z. Anorg. Allg. Chem.*, 2011, **637**, 901–906.

4 A. Ugrinov and S. C. Sevov, *J. Am. Chem. Soc.*, 2002, **124**, 10990–10991.

5 (*a*) L. Yong, S. D. Hoffmann and T. F. Fässler, *Z. Anorg. Allg. Chem.*, 2004, **630**, 1977–1981; (*b*) A. Ugrinov and S. C. Sevov, *Inorg. Chem.*, 2003, **42**, 5789–5791.

6 C. Downie, Z. Tang and A. M. Guloy, *Angew. Chem., Int. Ed.*, 2000, **39**, 337–340.

7 (*a*) G. S. Armatas and M. G. Kanatzidis, *Nature*, 2006, **441**, 1122–1125; (*b*) D. Sun, A. E. Riley, A. J. Cadby, E. K. Richmann, S. D. Korlann and S. H. Tolbert, *Nature*, 2006, **441**, 1126–1130; (*c*) M. M. Bentlohner, M. Waibel, P. Zeller, K. Sarkar, P. Muller Buschbaum, D. Fattakhova-Rohlfing and T. F. Fässler, *Angew. Chem., Int. Ed.*, 2015, **54**, 3748–3753.

8 A. Spiekermann, S. D. Hoffmann, T. F. Fässler, I. Krossing and U. Preiss, *Angew. Chem., Int. Ed.*, 2007, **46**, 5310–5313.

9 (*a*) M. M. Bentlohner, L.-A. Jantke, T. Henneberger, C. Fischer, K. Mayer, W. Klein and T. F. Fässler, *Chem. – Eur. J.*, 2016, **22**, 13946–13952; (*b*) S. Scharfe and T. F. Fässler, *Eur. J. Inorg. Chem.*, 2010, **8**, 1207–1213; (*c*) D. F. Hansen, B. B. Zhou and J. M. Goicoechea, *J. Organomet. Chem.*, 2012, **721–722**, 53–61.

10 (*a*) F. S. Geitner, W. Klein and T. F. Fässler, *Dalton Trans.*, 2017, **46**, 5796–5800; (*b*) L. Yong, M. B. Boeddinghaus and T. F. Fässler, *Z. Anorg. Allg. Chem.*, 2010, **636**, 1293–1296.

11 (*a*) C. Schenk and A. Schnepf, *Angew. Chem., Int. Ed.*, 2007, **46**, 5314–5316; (*b*) F. Henke, C. Schenk and A. Schnepf, *Dalton Trans.*, 2009, 9141–9145.

12 K. Mayer, L.-A. Jantke, S. Schulz and T. F. Fässler, *Angew. Chem., Int. Ed.*, 2017, **56**, 2350–2355.

13 M. S. Denning and J. M. Goicoechea, *Dalton Trans.*, 2008, 5882–5885.

14 (*a*) A. Nienhaus, R. Hauptmann and T. F. Fässler, *Angew. Chem., Int. Ed.*, 2002, **41**, 3213–3215; (*b*) M. B. Boeddinghaus, S. D. Hoffmann and T. F. Fässler, *Z. Anorg. Allg. Chem.*, 2007, **633**, 2338–2341.

15 B. B. Zhou, M. S. Denning, T. A. D. Chapman, J. E. McGrady and J. M. Goicoechea, *Chem. Commun.*, 2009, 7221–7727.

16 A. Spiekermann, S. D. Hoffmann, F. Kraus and T. F. Fässler, *Angew. Chem., Int. Ed.*, 2007, **46**, 1638–1640.

17 S. Joseph, M. Hamberger, F. Mutzbauer, O. Härtl, M. Meier and N. Korber, *Angew. Chem., Int. Ed.*, 2009, **48**, 8770–8772.

18 (*a*) M. M. Gillett-Kunnath, J. I. Paik, S. M. Jensen, J. D. Taylor and S. C. Sevov, *Inorg. Chem.*, 2011, **50**, 11695–11701; (*b*) J. M. Goicoechea and S. C. Sevov, *Angew. Chem., Int. Ed.*, 2005, **44**, 4026–4028; (*c*) V. Hlukhyy, S. Stegmaier, L. van Wullen and T. F. Fässler, *Chem. – Eur. J.*, 2014, **20**, 12157–12164.

19 E. N. Esenturk, J. Fettinger and B. Eichhorn, *Chem. Commun.*, 2005, 247–249.

20 G. Espinoza-Quintero, J. C. A. Duckworth, W. K. Myers, J. E. McGrady and J. M. Goicoechea, *J. Am. Chem. Soc.*, 2014, **136**, 1210–1213.

21 (*a*) X. Jin, G. Espinoza-Quintero, B. Below, V. Arcisauskaite, J. M. Goicoechea and J. E. McGrady, *J. Organomet. Chem.*, 2015, **792**, 149–153; (*b*) C. Liu, I. A. Popov, L. J. Li, N. Li, A. I. Boldyrev and Z. M. Sun, *Chem. – Eur. J.*, 2018, **24**, 699–705.

22 J. M. Goicoechea and S. C. Sevov, *J. Am. Chem. Soc.*, 2005, **127**, 7676–7677.

23 (*a*) V. Hlukhyy, H. He, L.-A. Jantke and T. F. Fässler, *Chem. – Eur. J.*, 2012, **18**, 12000–12007; (*b*) H. He, W. Klein, L.-A. Jantke and T. F. Fässler, *Z. Anorg. Allg. Chem.*, 2014, **640**, 2864–2870.

24 S. Scharfe, T. F. Fässler, S. Stegmaier, S. D. Hoffmann and K. Ruhland, *Chem. – Eur. J.*, 2008, **14**, 4479–4483.

25 (*a*) J. Q. Wang, S. Stegmaier and T. F. Fässler, *Angew. Chem., Int. Ed.*, 2009, **48**, 1998–2002; (*b*) B. Zhou, M. S. Denning,

D. L. Kays and J. M. Goicoechea, *J. Am. Chem. Soc.*, 2009, **131**, 2802–2803.

26 (*a*) E. N. Esenturk, J. Fettinger, Y. F. Lam and B. Eichhorn, *Angew. Chem., Int. Ed.*, 2004, **43**, 2132–2134; (*b*) E. N. Esenturk, J. Fettinger and B. Eichhorn, *J. Am. Chem. Soc.*, 2006, **128**, 9178–9186; (*c*) B. B. Zhou, T. Kramer, A. L. Thompson, J. E. McGrady and J. M. Goicoechea, *Inorg. Chem.*, 2011, **50**, 8028–8037.

27 J.-Q. Wang, S. Stegmaier, B. Wahl and T. F. Fassler, *Chem. – Eur. J.*, 2010, **16**, 1793–1798.

28 E. N. Esenturk, J. C. Fettinger and B. W. Eichhorn, *J. Am. Chem. Soc.*, 2006, **128**, 12–13.

29 B. Kesanli, E. J. Halsig, P. Zavalij, Y. F. Lam and B. W. Eichhorn, *J. Am. Chem. Soc.*, 2007, **129**, 4567–4574.

30 C. Liu, X. Jin, L.-J. Li, J. Xu, J. E. McGrady and Z.-M. Sun, *Chem. Sci.*, 2019, **10**, 4394–4401.

31 (*a*) Z. M. Sun, H. Xiao, J. Li and L. S. Wang, *J. Am. Chem. Soc.*, 2007, **129**, 9560–9561; (*b*) F. S. Kocak, P. Zavalij, Y. F. Lam and B. W. Eichhorn, *Inorg. Chem.*, 2008, **47**, 3515–3520.

32 S. Mitzinger, L. Broeckaert, W. Massa, F. Weigend and S. Dehnen, *Nat. Commun.*, 2016, **7**, 10480.

33 C. Liu, L.-J. Li, X. Jin, J. E. McGrady and Z.-M. Sun, *Inorg. Chem.*, 2018, **57**, 3025–3034.

34 J. M. Goicoechea and S. C. Sevov, *J. Am. Chem. Soc.*, 2006, **126**, 4155–4161.

35 M. M. Gillett-Kunnath, J. I. Paik, S. M. Jensen, J. D. Taylor and S. C. Sevov, *Inorg. Chem.*, 2011, **50**, 11695–11701.

36 (*a*) O. V. Dolomanov, L. J. Bourhis, R. J. Gildea, J. A. K. Howard and H. J. Puschmann, *Appl. Crystallogr.*, 2009, **42**, 339–341; (*b*) G. M. Sheldrick, *Acta Crystallogr., Sect. A: Found. Crystallogr.*, 2008, **64**, 112–122; (*c*) G. M. Sheldrick, *Acta Crystallogr., Sect. C: Struct. Chem.*, 2015, **71**, 3–8.

37 F. Neese, ORCA 4.0, *Wiley Interdiscip. Rev.: Comput. Mol. Sci.*, 2018, **8**, e1327.

38 (*a*) A. D. Becke, *Phys. Rev. A*, 1988, **38**, 3098–3100; (*b*) J. P. Perdew, *Phys. Rev. B: Condens. Matter Mater. Phys.*, 1986, **33**, 8822–8824.

39 (*a*) F. Weigend and R. Ahlrichs, *Phys. Chem. Chem. Phys.*, 2005, **7**, 3297–3305; (*b*) J. Zheng, X. Xu and D. G. Truhlar, *Theor. Chem. Acc.*, 2011, **128**, 295–305.

40 B. Metz, H. Stoll and M. Dolg, *J. Chem. Phys.*, 2000, **113**, 2563–2569.

41 F. Neese, *J. Comput. Chem.*, 2003, **24**, 1740–1747.

42 F. Weigend, *Phys. Chem. Chem. Phys.*, 2006, **8**, 1057–1065.

43 V. Barone and M. Cossi, *J. Phys. Chem. A*, 1998, **102**, 1995–2001.

44 K. Zeckert, *Dalton Trans.*, 2012, **41**, 14101–14106.

45 B. Cordero, V. Gómez, A. E. Platero-Prats, M. Revés, J. Echeverría, E. Cremades, F. Barragán and S. Alvarez, *Dalton Trans.*, 2008, 2832–2838.

46 F. K. Sheong, W.-J. Chen, J.-X. Zhang, Y. Li and Z. Lin, *Dalton Trans.*, 2017, **46**, 2214–2219.

47 J.-Q. Wang, B. Wahl and T. F. Fässler, *Angew. Chem., Int. Ed.*, 2010, **49**, 6592–6595.